Effect of masking phase-only holograms on the quality of reconstructed images

YUANBO DENG,[1] DAPING CHU[1,*]

[1]Photonics and Sensors Group, Department of Engineering, University of Cambridge, 9 JJ Thomson Avenue, Cambridge, CB3 0FA, UK

*Corresponding author: dpc31@cam.ac.uk

Received XX Month XXXX; revised XX Month, XXXX; accepted XX Month XXXX; posted XX Month XXXX (Doc. ID XXXXX); published XX Month XXXX

A phase-only hologram modulates the phase of the incident light and diffracts it efficiently with low energy loss because of the minimum absorption. Much research attention has been on how to generate phase-only holograms, and little work has been done to understand the effect and limitation of their partial implementation possibly due to physical defects and constrains, in particular as in the practical situations where a phase-only hologram is confined or need to be sliced or tiled. The present study simulates the effect of masking phase-only holograms on the quality of reconstructed images in three different scenarios with different filling factors, filling positions and illumination intensity profiles. Quantitative analysis confirms that the width of the image point spread function becomes wider and the image quality decreases, as expected, when the filling factor decreases, and the image quality remains the same for different filling positions as well. The width of the image point spread function as derived from different filling factors shows a consistent behaviour to that as measured directly from the reconstructed image, especially as the filling factor becomes small. Finally mask profiles of different shapes and intensity distributions are shown to have more complicated effects on the image point spread function, which in turn affects the quality and textures of the reconstructed image.

OCIS codes: *(090.1705) Computer holography; (090.2870) Holography displays; (110.3000) Image quality assessment*

http://dx.doi.org/10.1364/AO.99.099999

1. INTRODUCTION

Phase-only hologram is one kind of diffractive optical elements (DOEs), which could diffract an incident beam to desired positions, reconstructing holographic patterns or images. Compared with amplitude hologram, phase-only hologram modulates the phase of an incident beam for high diffraction efficiency [1]. It has been widely used in various applications such as holographic displays [2-4], holographic optical switches [5,6], wavefront compensations [7], and holographic optical tweezers [8,9]. Researches have been done to develop optimized algorithms to calculate phase-only holograms for specific required target patterns or images, by balancing the image quality and computation power needed. For example, simulated annealing and direct binary search are more efficient if the target pattern is in a simple case, like a point or a few points [10-12]. However, if the target image is more complicated, iterative algorithms such as the Gerchberg-Saxton (G-S) algorithm are more efficient [13]. For the G-S algorithm, the target image pixel number is equal to the spatial pixel number of the hologram plane, which allows the use of fast Fourier transform (FFT) in each iteration. The result converges to an optimized phase-only hologram after certain iterations. Some other algorithms have been developed based on the G-S algorithm, such as Fienup [14] and Fienup with don't care area (Fidoc)[15,16]. Fienup provides amplitude feedback during each iteration to achieve faster convergence and Fidoc adds areas around the target image for better quality of the reconstructed image. These foregoing researches have been focused on how to calculate the right phase-only hologram, however, it may face some issues when the phase-only hologram is been used in certain practical situations.

A phase-only hologram is usually calculated assuming the incident beam is a plane wave or Gaussian wave, but the actual incident beam profile and size might be different from the ideal case, thus affecting the quality of reconstructed images. Phase-only hologram is usually loaded on a phase-only spatial light modulator (SLM). In addition, SLM has a large size such as HD (1920*1080) or even 4K in the near future. To calculate such a large hologram can be very time consuming. Therefore, slicing and tiling hologram would become a valuable approach to improve the calculation efficiency. Furthermore, we may use

a single SLM to load a tiled hologram for different channels (for example, R, G, and B channels in a full color holographic display) to reduce the apparatus costs. Meanwhile, some algorithms require the hologram to be sliced or tiled for a specific purpose [17-19]. All these can be treated as equivalent to adding a mask to phase-only holograms, which will unavoidably affect the quality of reconstructed images.

A preliminary attempt was made to look at a limited scope of the mask filling factor effect [20], while in this paper, how the mask related factors influence the quality of reconstructed images will be systematically analyzed, with different filling factors, filling positions and illumination intensity profiles. All these factors have direct impacts on the effective utilization of a phase-only hologram, thus affecting the quality of the reconstructed image.

2. THEORY AND METHODS

A. Algorithm

G-S algorithm is an iterative phase retrieval method with fast convergence and the quality of the reconstructed image is normally good. It is widely used in different holographic applications [2-4,8,9]. It also forms the base for several other popular algorithms [14-16,19,21]. We use G-S calculated phase-only holograms to reconstruct the target images and two metrics, root mean square error (RMSE) and structural similarity (SSIM) [22], to evaluate the reconstructed image quality. RMSE is the measurement of the difference between the values predicted by an estimator (target image) and the values actually observed (reconstructed image). While SSIM is a method for measuring the similarity between two images for the fact that the inter-dependencies between pixels especially when they are spatially close carry important information about the structure of a visualized image.

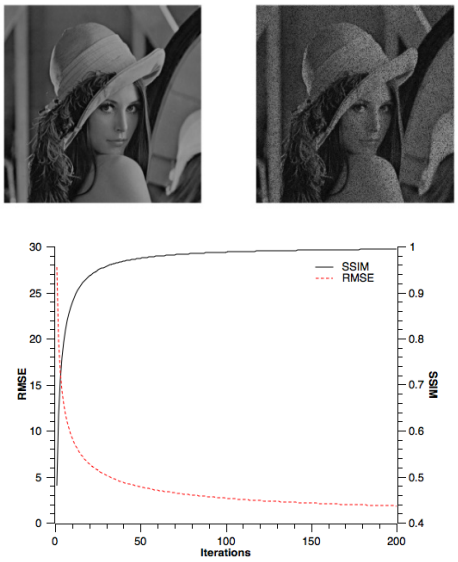

Fig. 1. (a) Target image, (b) Reconstructed image using G-S algorithm after 100 iterations and (c) RMSE and SSIM values vs the number of iterations.

We run different iterations of G-S algorithm to calculate the phase-only hologram with the same target image shown in Fig. 1(a). The reconstructed image is shown in Fig. 1(b), and the relationship between RMSE and SSIM of the reconstructed image and the number of iterations is shown in Fig. 1(c). It is shown that G-S algorithm converges fast. After only several time of iterations, the change of the generated hologram slows down significantly. At 100 times of iteration, RMSE=2.66 and SSIM=0.988, indicating a very high quality of the reconstructed image [23]. In following simulations, all the phase-only holograms will be calculated using G-S algorithm with 100 iterations.

B. Aperture characteristics

Let us consider an illuminated phase-only hologram $h(x,y)$

$$h(x,y) = A(x,y)\exp(i\phi(x,y)) \quad \textbf{(1)}$$

where the phase term $\phi(x,y)$ represents the target image information and the amplitude term $A(x,y)$ reflects the amplitude profile of the incident beam. If illuminated by a plane wave, $A(x,y)$=1. When a mask $p(x,y)$ is added on the illuminated hologram plane, the resultant hologram can be expressed as

$$\tilde{h}(x,y) = h(x,y) * p(x,y) \quad \textbf{(2)}$$

where $*$ denotes the multiplication operation and the corresponding reconstructed image as the Fourier transform F of Eq. (2) is

$$\tilde{H}(u,v) = \mathcal{F}\left\{\tilde{h}(x,y)\right\} = \mathcal{F}\left\{h(x,y) * p(x,y)\right\}$$
$$= H(u,v) \otimes P(u,v) \quad \textbf{(3)}$$

where $\otimes$ denotes the convolution operation, $H(u,v)$ and $P(u,v)$ are the Fourier transform of $h(x,y)$ and $p(x,y)$ respectively. The new reconstructed image is the original reconstruction image $H(u,v)$ convolved with the Fourier transformed mask $P(u,v)$.

In most applications, a computer generated hologram (CGH) is loaded on a pixelated phase-only SLM, and the effective hologram $t(x,y)$ on the device can be expressed by

$$t(x,y) = pa \otimes [comb * h(x,y)] \quad \textbf{(4)}$$

where pa is the aperture of each pixel and $comb$ a comb function which presents the periodic structure of SLM. In this study, the focus is on the first order of diffraction and the filling factor of each pixel is set to be 100% for simplicity. For normal SLMs such as phase-only liquid crystal on silicon (LCoS) devices [24], the pixel aperture pa is square or rectangular, and we define the pixel dimensions as a_x, a_y and pixel pitch as p_x , p_y (=a_x, a_y ,for 100% pixel filling factor), the effective hologram is shown as

$$t(x,y) = rect(\frac{x}{a_x},\frac{y}{a_y}) \otimes \left\{\frac{1}{p_x p_y} comb(\frac{x}{p_x},\frac{y}{p_y}) * h(x,y)\right\} \quad \textbf{(5)}$$

Consequently the reconstructed image of $t(x,y)$ can be expressed as

$$T(u,v) = \mathcal{F}\left\{t(x,y)\right\}$$
$$= a_x a_y \mathrm{sinc}(ua_x, va_y)\left\{comb(up_x, vp_y) \otimes H(u,v)\right\} \quad \textbf{(6)}$$

If a mask is applied to the effective hologram, according to Eqs. (1)-(3), the final reconstructed image will be:

$$\tilde{T}(u,v) = \mathcal{F}\{t(x,y) * p(x,y)\} = T(u,v) \otimes P(u,v)$$

$$= a_x a_y \mathrm{sinc}(ua_x, va_y)[comb(up_x, vp_y) \otimes H(u,v)] \otimes P(u,v) \quad (7)$$

Usually, a mask has a shape of square (rectangular), circular, or Gaussian. For example, when the hologram is illuminated by a plane wave covering the full area of the hologram, the mask is square or rectangular with the overall size of the SLM L_x, L_y. In this case, the Fourier transform of the mask is a sinc function:

$$P_{rec}(u,v) = L_x L_y \mathrm{sinc}(uL_x, vL_y) \quad (8)$$

For a circular mask profile of radius r, the Fourier transform of the mask is a first order Bessel function, which can be expressed as:

$$P_{cir}(u,v) = \frac{rJ_1(2\pi r\sqrt{u^2+v^2})}{\sqrt{u^2+v^2}} \quad (9)$$

For a Gaussian mask profile with the variance σ, the Fourier transform is still a Gaussian profile:

$$P_{gau}(u,v) = e^{-2\pi^2\sigma^2(u^2+v^2)} \quad (10)$$

The above examples show that in general if a hologram could reconstruct an ideal image point, applying a mask to it would result in a spatially extended feature known as the point spread function (PSF) of such a combination. For all these three types of masks, the Fourier transform of a mask is close to a δ function when the mask size is large, which means that the width of the PSF is small. On the other hand, when the mask size decreases, the width of the corresponding PSF will increase and the sharpness and hence the quality of the reconstructed image will decrease. Furthermore, if a PSF has side robes (tails), the resultant intensity of two closely positioned features on the reconstructed image will interfere with each other thus causing speckles [24]. The degree of speckles will depend on the coherency of the illumination beam. The principle is illustrated in Fig.2.

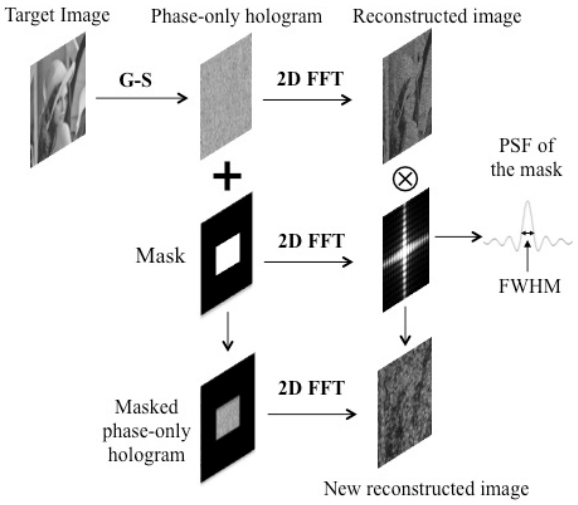

Fig. 2. The reconstruction of the masked hologram is equal to the original phase-only hologram convolved with the Fourier transform of the mask.

3. RESULTS AND DISCUSSIONS

A. Mask size (filling factor)

We investigate the relationship between the quality of reconstructed images and the mask size (also known as the filling factor). Here we define the filling factor μ as the ratio of the information quantity being used, H_{mask}, to the overall information quantity of the whole hologram, $H_{overall}$, as expressed in Eq. (11).

$$\mu = \frac{H_{masked}}{H_{overall}} \quad (11)$$

For the mask with a uniform intensity distribution, the filling factor is proportional to the mask dimension. While for the mask with a non-uniform intensity distribution such as Gaussian profile, the filling factor is more appropriate to describe the mask than the mask dimension. Therefore, the filling factor is applied to evaluate the effect for different masks. If we consider a mask in the shape of a square with a length L is added to a phase-only hologram, the filling factor μ can be expressed as

$$\mu \propto L^2 \quad (12)$$

According to Eq. (8), the Fourier transform of a square mask is a 2D sinc function. We define the full width half maximum (FWHM) of the central order of the 2D sinc function as the width of the corresponding point spread function, ΔPSF_{mask}. According to Eq. (8) and Eq. (12), we can get the relation between ΔPSF_{mask} and μ as:

$$\Delta PSF_{mask} = \frac{C}{\sqrt{\mu}} \quad (13)$$

where C is a constant. We can see that ΔPSF will increase when μ decreases. To evaluate the effect of the filling factor on the reconstructed image, we use a 8×8 checkerboard image of 512×512 pixels shown in Fig. 3 as the target image with square masks of different filling factors from 100% to 1% by 1%.

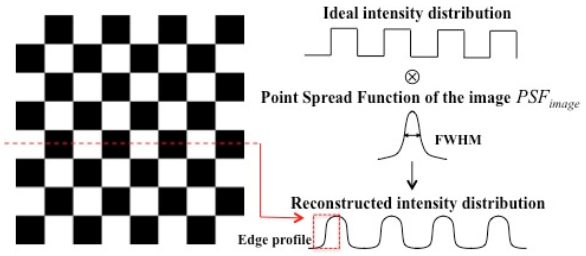

Fig. 3 Phase-only hologram of the checkerboard target image is obtained and then reconstructed. The average cross-section intensity distribution of one row consisting of black and white square block is calculated. Instead of sharp step profile, the edge profile is spread to some extent, which could be considered as the convolution of the ideal intensity distribution and a point spread function PSF_{image}.

For each μ, the calculation process is to: (i) add the corresponding mask to the hologram, (ii) apply 10 times

zero-padding of the phase-only hologram in order to reveal details and speckles of corresponding reconstructed image as described in Refs. [19] and [21], (iii) reconstruct the hologram, (iv) get the average cross-section intensity distribution of one row consisting of black and white square block, and (v) calculate the intensity distribution curve from the high value (white block) to the low value (black block) as the edge profile to show the spread out of the sharp edge of the target image.

The reconstructed checkerboard images with filling factor 100%, 50%, 20%, 10%, 5%, 2% and 1% are shown in Fig. 4(a), where only the central 4 blocks are presented to show the details of the reconstructed images. It can be seen from Fig. 4(a) that the quality of the reconstructed image reduces gradually as μ decreases to 20%. However, when μ decreases further, the quality of reconstructed image decreases rapidly.

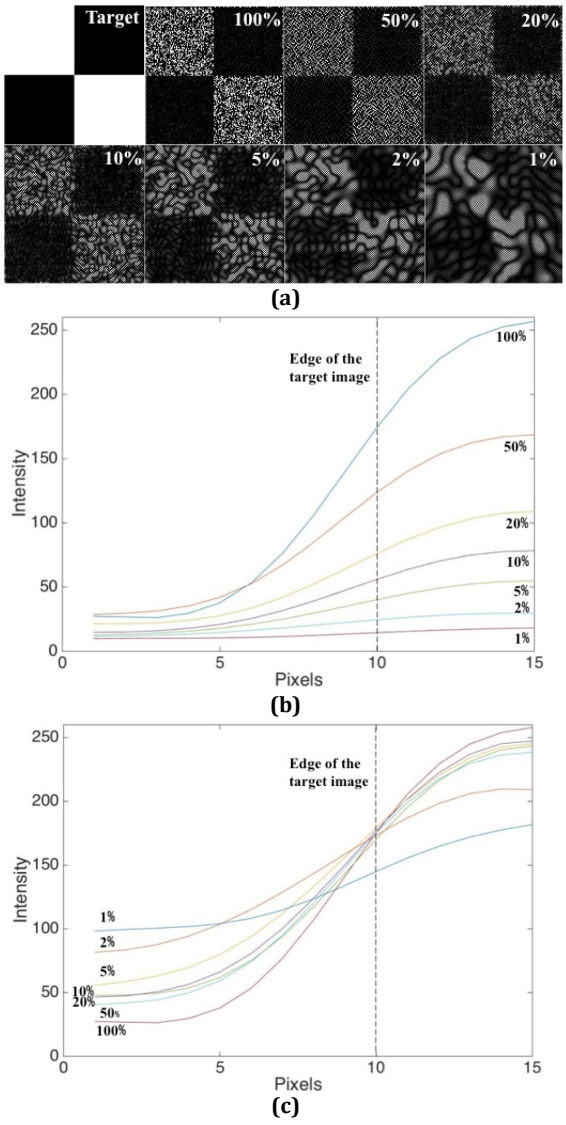

Fig.4 (a) Central 4 blocks of the reconstructed checkerboard image with μ=100%, 50%, 20%, 10%, 5%, 2% and 1% as indicated; (b) the edge profile between the first white and black block is obtained to see the changes; (c) the curves of (b) as normalized by energy.

To quantitatively analyze the change of image quality, we calculated the cross-section intensity profile averaged over one row (Row 5) of the checkerboard, and plotted it across one white/black boundary (indicated as the edge profile in Fig. 3) in Fig. 4(b). We can see clearly that when μ decreases, the intensity drops accordingly in both the white and black parts and the white part drops more rapidly than the black part. To illustrate clearly this trend, intensity profiles normalized to the same energy are shown in Fig. 4(c) for different filling factors. We can find that the edge profile spreads out more evenly as the filling factor decreases. This can be regarded as the original sharp edge of the target image convolved with a PSF of the reconstructed image as illustrated in Fig. 3 as PSF_{image} .

Deconvolution of the reconstructed intensity distribution to the ideal intensity distribution can be used to calculate PSF_{image}, and we could define the FWHM of PSF_{image} as ΔPSF_{image}. PSF_{image} may differ from PSF_{mask} as illustrated in Fig. 2, and the comparison of ΔPSF_{image} with ΔPSF_{mask} is shown in Fig.5.

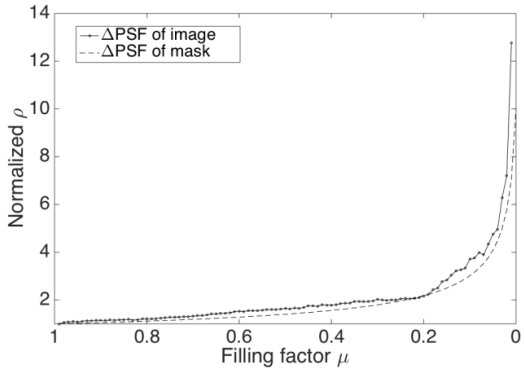

Fig.5 The real curve shows the values of ΔPSF_{image} for filling factor μ changing from 100% to 1%. Dashed curve is the theoretical value between μ and ΔPSF_{mask}. The two lines are normalized and the results show that they are consistent with each other.

We can see that ΔPSF_{image} *and* ΔPSF_{mask} agree with each other and they increase slowly when μ is larger than 0.2 and then increase rapidly when μ is smaller than 0.2. However, it shows that the curve of ΔPSF_{image} is always above the curve of ΔPSF_{mask}, which might due to the fact that in actual situations, the side robes of the sinc function will interfere with each other between two spatial pixels, thus creating speckles. The average of the edge intensity profile will decrease the effects of speckles, however it still degrades the quality of reconstructed image. Therefore, the actual ΔPSF_{image} will be larger than ΔPSF_{mask}, especially when μ is very small.

As we can see in Fig. 4(a), if ΔPSF_{image} increases, the quality of reconstructed image will decrease, we use the Lena image in Fig. 1(a) and RMSE as well as SSIM to quantitatively evaluate the changes in quality of reconstructed image. As shown in Fig. 6, it is clear that when we use the full hologram, the reconstructed image is of good quality with RMSE=2.66 and SSIM=0.988. However as μ decreases, RMSE value starts to increase and SSIM value starts to drop, representing the drop of the reconstructed image quality as we expected.

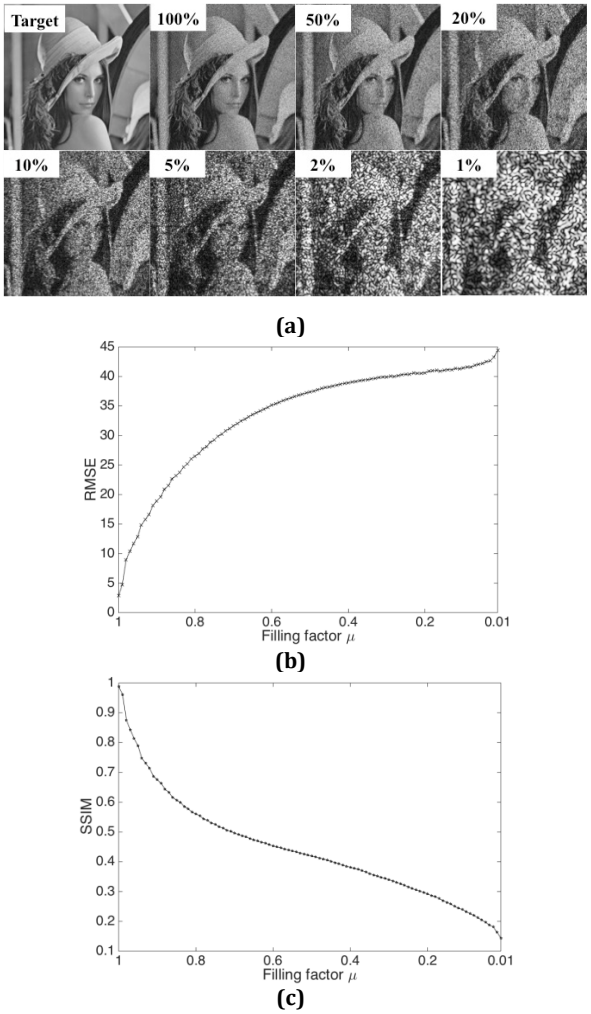

Fig.6 (a) Reconstructed Lena images for filling factor 100%, 50%, 20%, 10%, 5%, 2% and 1%; (b) and (c) RMSE and SSIM values of the reconstructed image, respectively.

The relation between filling factor and image quality assessed by RMSE and SSIM is not as the same as the relation between filling factor and ΔPSF , this is because the effects of the masking is dependent on the specific contents of the reconstructed image, which means for different reconstructed image, the changing trend of RMSE and SSIM might be different. However, it still shows the general trend that when μ is large, the variation is small, while μ is very small, it changes more rapidly.

B. Mask filling position

If we take the Fourier transform of a 2D image, the low frequency components of the amplitude information are distributed in the center on the Fourier plane, while the high frequency ones are away from the center. In this case, if we add a finite size mask on the Fourier plane at different filling positions and then take the inverse Fourier transform, the reconstructed image will vary correspondingly. Different from that, the phase term of a phase-only hologram carries the information of reconstructed image and its distribution is optimized by iterative algorithms. We would like to apply the same mask at different filling positions to it and evaluate the quality of reconstructed image to see if different parts of the phase-only hologram play the same role of reconstructing the target image.

We calculate a phase-only hologram of 512*512 from the Lena image in Fig. 1(a) and then divide the hologram into 16 pieces of equal size. Subsequently we choose each piece individually and set the rest with blank information before reconstruction. This can be regarded as masking the original hologram with a mask of the same filling factor 6.25% but at different filling positions without overlaps. The quality of reconstructed images in terms of RMSE and SSIM is shown in Fig. 7. We can see that they remain to be almost constant for different filling positions. This means that, unlike the Fourier transformed amplitude information of a 2D image, a phase-only hologram is mask filling position insensitive. This conclusion also applies to the masks used in normal working situations with a larger filling factor than what is used here, as they can be regarded as a combination of smaller masks.

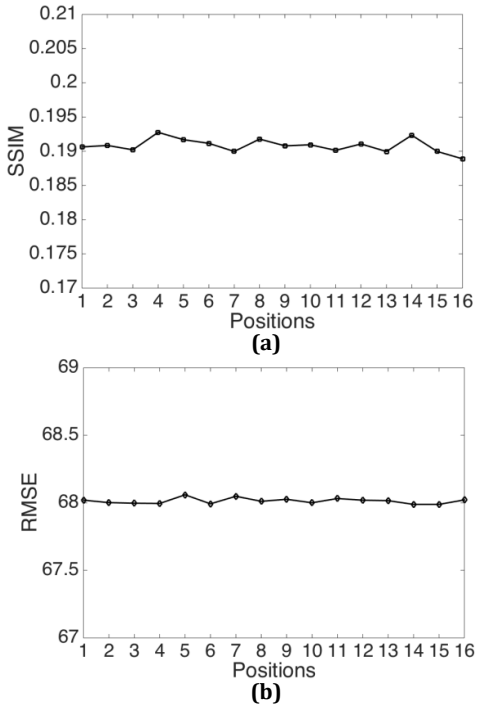

Fig.7 (a) RMSE values of reconstructed images for the same phase-only hologram with masks at different filling positions; (b) SSIM values of reconstructed images for the same phase-only hologram with masks at different filling positions.

C. Mask illumination intensity profile

Now we investigate how the mask illumination intensity profile influence the quality of reconstructed image. We reconstruct the phase-only hologram of the same checkerboard image as in Fig. 3 and apply masks with the same filling factor but different mask illumination intensity profiles: uniformly illuminated square, circle, and border shapes, plus a Gaussian distribution and a real laser beam, as shown in the second row in Fig. 8. To illustrate the effect of the mask illumination profile clearly, a rather low filling factor μ=0.1 is used in all cases. With a low filling factor,

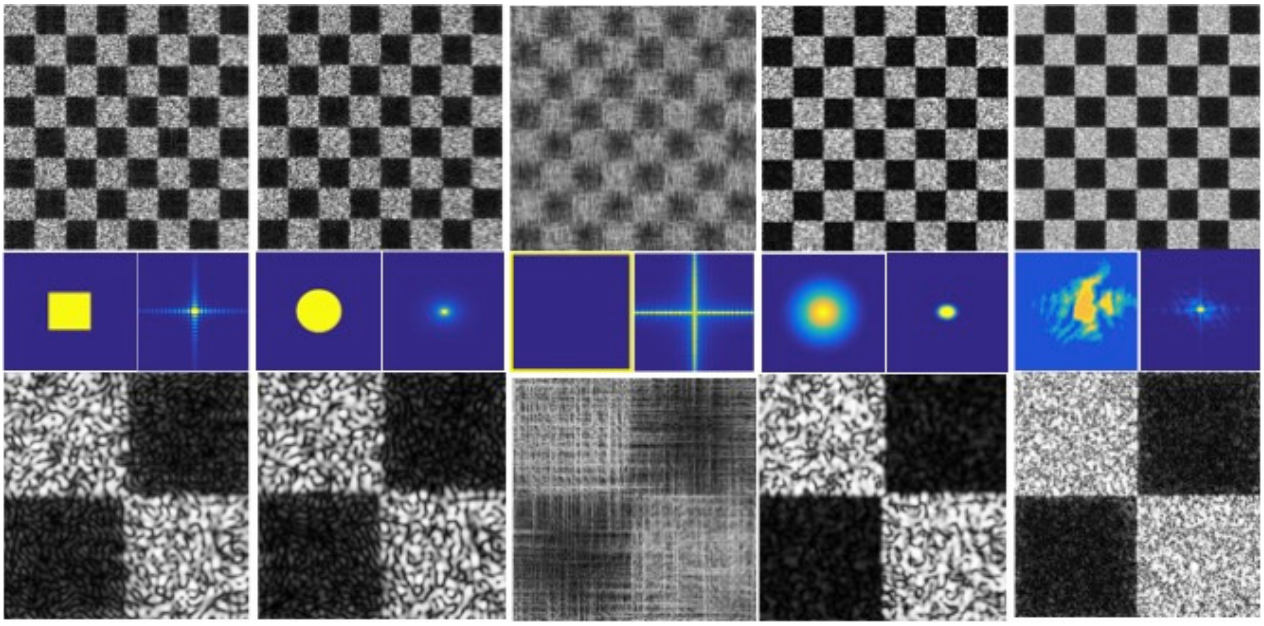

(a) **(b)** **(c)** **(d)** **(e)**

Fig.8 (a) Top image is the reconstructed image of checkerboard with square mask, middle left is the square mask with μ=0.1, middle right is the Fourier transform of the square mask, bottom image is the center four bricks of the top image to show the details. From (b) to (e) are the similar situations for circular, border, Gaussian and a real laser beam, respectively.

the masking effect is more obvious while the reconstructed image can still be distinguished. As shown in Fig. 8(a) and Fig. 8(b), respectively, the Fourier transforms of a uniformly illuminated square and a circular mask profiles are 2D sinc and 2D Bessel function, where most of the intensity is distributed in the central order but there are also higher orders resulting in intensity oscillation away from the center.

Oscillations between spatial pixels will interfere with each other thus changing the texture of the reconstructed image, creating speckles. Furthermore, because of the oscillations, the edge between the high value (white) and the low value (black) is not very clear, so we could see some white spots spreading into the black part as shown in the bottom images of Fig. 8(a) and Fig. 8(b). This phenomenon becomes more obvious for the Fourier transform of the uniformly illuminated border mask profile as shown in Fig. 8(c) where the intensity is evenly distributed in the central order and higher orders. Therefore, the interference between pixels become more pronounced in the reconstructed image, and the resultant quality and texture of the reconstructed image are worse compared with other profiles of the same filling factor. While for the Gaussian mask profile in Fig. 8(d), as the Fourier transform of a Gaussian distribution is still a Gaussian distribution (Eq. (10)), there are less interferences and the edge between white and black in the reconstructed image is sharper than the others. Finally, we apply a real laser beam profile [25] as shown in Fig. 8(e) for the same filling factor. The laser beam profile is not well focused, therefore it has a larger spatial dimension than the other profiles and a smaller central robe width of its Fourier transform. Its oscillations in the Fourier plane are irregular, thus making the texture in the white part much smoother that the others and the edge between white and black better than the uniformly illuminated ones but not than that of the Gaussian profile mask.

It can be summarized that for different mask illumination intensity profiles with the same filling factor, the texture and quality of reconstructed images depends on the nature of the Fourier transform of the mask profile. Strong oscillations in the Fourier transform function especially the high frequency part will affect the quality and texture of the reconstructed image and create speckles in the white region and noises in the black region, while weak and few oscillations result in smooth white regions with sharp edges and low noise in the black region. Finally, the dimension of the profile especially the low frequency part will affect the texture of the reconstructed in the part, and smaller in dimension will cause more speckles.

4. CONCLUSIONS

The above studies concern the effect of masking a phase-only holograms on the reconstructed images. Quantitatively evaluations were carried out for different masking scenarios, including when the phase-only hologram is illuminated by an incident beam with an arbitrary profile and size, or when the phase-only hologram is sliced and then tiled up for reducing the computational load but with acceptable quality. This has practical value when it is necessary to use the phase-only hologram on a SLM efficiently.

Based on the above results, it can be concluded that: (1) if a mask is added onto a phase-only hologram, the reconstructed image will be the original one convolved with the Fourier transform of the mask; (2) the mask filling position has no influence on the quality of the reconstructed image; (3) the mask filling factor defines the FWHM of the point spread function of its Fourier transform as well as of the reconstructed image and the decrease of the mask filling factor will result in the increase of the FWHM of the pixel point spread function increases and the decrease of the quality of the reconstructed image; (4) the mask illumination intensity profile will affect the texture and details of the reconstructed image, especially when the filling factor value is low.

It is worth to point out that although the phase-only hologram is calculated as a matrix without the actual size information, the general principle and approach used in this paper apply to all pixel sizes. Different pixel size and the pixelated structure of an SLM will only change the reconstructed image size and result in high orders, which will not affect the conclusions of this paper.

For future work, focus will be on how the phase variations and phase noises influence the reconstruction of phase-only hologram, which is important in practical applications such as holographic projection displays [2-4], wavefront encoding for telecom [26] and calibration in start imaging [27-28].

Acknowledgement. The authors would like to thank the UK Engineering and Physical Sciences Research Council (EPSRC) for the support through the Platform Grant for Liquid Crystal Photonics (EP/F00897X/1).

Reference

1. H. Dammann and K. Görtler, "High-efficiency in-line multiple imaging by means of multiple phase holograms", Optics communications 3, 312-315 (1971).
2. N. Collings, M. Reufer, R.V. Penty, B. Sumpf, M.Safer, D.P. Chu and W.A. Crossland, "Holographic projection based on tapered lasers and nematic liquid crystal on silicon device", Proc.SPIE-7775,777504-1 (2010).
3. J.-S. Chen, Q. Smithwick, and D. Chu, "Implementation of shading effect for reconstruction of smooth layer-based 3D holographic images", Proc. SPIE-8648, 86480R–9 (2013).
4. F. Yaraş, H. Kang, and L. Onural, "Real-time phase-only color holographic video display system using LED illumination", Applied Optics 48, H48-H53 (2009).
5. W.A. Crossland, I.G. Manolis, M.M. Redmond, K.L. Tan, T.D. Wilkinson, M.J. Holmes, T.R. Parker, H.H. Chu, J. Croucher, V.A. Handerek, S.T. Warr, B. Robertson, I.G. Bonas, R. Franklin, C. Stace, H.J. White, R.A. Woolley, and G. Henshall, "Holographic optical switching: the "ROSES" demonstrator", Journal of Lightwave Technology 18, 1845–1854 (2000).
6. L. Workshop, A. T. Park, G. Baxter, S. Frisken, D. Abakoumov, H. Zhou, I. Clarke, A. Bartos, and S. Poole, "Highly programmable Wavelength Selective Switch based on Liquid Crystal on Silicon switching elements", OFC 2006.
7. F. Li, J. Zhao, R. Li, B. Zhang, L. Zheng, and X. Zhang, "Design and fabrication of CGH for aspheric surface testing and its experimental comparison with null lens", Proc. SPIE-7656, 765643–1(2010).
8. J.E. Curtis, B.A. Koss, and D.G. Grier, "Dynamic holographic optical tweezers", Optics Communications 207, 169-175 (2002).
9. G. Sinclair, J. Leach, P. Jordan, G. Gibson, E. Yao, Z.J. Laczik, M.J. Padgett, and J. Courtial. "Interactive application in holographic optical tweezers of a multi-plane Gerchberg-Saxton algorithm for three-dimensional light shaping", Optics Express 12, 1665-1670 (2004).
10. S. Kirkpatrick, C.D. Gelat, and M.P. Vecchi, "Optimisation by simulated annealing", Science 220, 671-80 (1971).
11. M.A. Seldowitz, J.P. Allebach and D.W. Sweeney, "Synthesis of digital holograms by direct binary search", Appl. Opt. 26, 2779–98 (1987).
12. A. Kirk and T. Hall, "Design of binary computer generated holograms by simulated annealing: coding density and reconstruction error", Opt. Commun. 94, 491–6 (1992).
13. R.W. Gerchberg, "A practical algorithm for the determination of phase from image and diffraction plane pictures", Optik 35, 237 (1972).
14. J.R. Fienup, "Reconstruction of an object from the modulus", Optics Letters 3, 27–29 (1978).
15. F. Wyrowski, "Diffractive optical elements: iterative calculation of quantized, blazed phase structures", Journal of the Optical Society of America A **7**, 961 (1990).
16. H. Akahori, "Spectrum leveling by an iterative algorithm with a dummy area for synthesizing the kinoform", Applied Optics 25, 802–11 (1986).
17. T. Haist, M.Schönleber, and H.J. Tiziani, "Computer-generated holograms from 3D-objects written on twisted-nematic liquid crystal displays", Optics Communications 140, 299-308 (1997).
18. A.J. Waddie, and M.R. Taghizadeh, "Interference effects in far-field diffractive optical elements", Applied Optics 38, 5915-5919 (1999).
19. J.S. Liu, N. Collings, W.A. Crossland, D.P. Chu, A. Waddie, and M.R. Taghizadeh, "Simulation and experiment on generation of an arbitrary array of intense spots by a tiled hologram", Journal of Optics 12, 085402 (2010).
20. Y. Deng and D. Chu, "Filling factor characteristics of masking phase-only hologram on the quality of reconstructed images", Proc.SPIE-9771,97710M (2016)
21. A. Georgiou, J. Christmas, N. Collings, J. Moore and W.A. Crossland, "Aspects of hologram calculation for video frames", Journal of Optics A: Pure and Applied Optics 10, 035302 (2008).
22. Z. Wang, A.C. Bovik, H.R. Sheikh, and E.P. Simoncelli, "Image quality assessment: from error visibility to structural similarity", IEEE Transactions on Image Processing 13, 600–12 (2004).
23. H.R. Sheikh, Z. Wang, L. Cormack and A.C. Bovik, "LIVE Image Quality Assessment Database Release 2", http://live.ece.utexas.edu/research/quality
24. Z. Zhang, Z. You, and D. Chu, "Fundamentals of phase-only liquid crystal on silicon (LCOS) devices", Light: Science & Applications 3, e213 (2014).
25. C.B. Roundy, "Current technology of laser beam profile measurements",http://wwwferp.ucsd.edu/LASERLAB/TUTOR/profile-tutorial.pdf
26. B. Robertson, Z. Zhang, M.M. Redmond, N. Collings, J. Liu, R.S. Lin, A.M. Jeziorska-Chapman, J.R. Moore, W.A. Crossland, and D.P. Chu, "Use of wavefront encoding in optical interconnects and fiber switches for crosstalk mitigation", Applied Optics 51, 659-668 (2012).
27. G. Wang, F. Xing, M. Wei, and Z. You, "Precision enhancement method for multiplexing image detector-based sun sensor with varying and coded apertures", Applied Optics 54,10467-10472 (2015).
28. F. Xing, Z. You, G. Zhang, and J. Sun, "A novel active pixels sensor (APS) based sun sensor based on a feature extraction and image correlation (FEIC) technique", Measurement Science and Technology 19, 125203 (2008).